Exploring Spatial Generalized Functional Linear Models: A Comparative Simulation Study and Analysis of COVID-19

Sooran Kim[a,*], Mark S. Kaiser[a], Xiongtao Dai[b]

[a]*Department of Statistics, Iowa State University, 2438 Osborn Dr, Ames, 50011-1090, Iowa, USA*
[b]*Division of Biostatistics, School of Public Health, University of California, Berkeley, 2121 Berkeley Way, Berkeley, 94720-7360, California, USA*

Abstract

Implementation of spatial generalized linear models with a functional covariate can be accomplished through the use of a truncated basis expansion of the covariate process. In practice, one must select a truncation level for use. We compare five criteria for the selection of an appropriate truncation level, including AIC and BIC based on a log composite likelihood, a fraction of variance explained criterion, a fitted mean squared error, and a prediction error with one standard error rule. Based on the use of extensive simulation studies, we propose that BIC constitutes a reasonable default criterion for the selection of the truncation level for use in a spatial functional generalized linear model. In addition, we demonstrate that the spatial model with a functional covariate outperforms other models when the data contain spatial structure and response variables are in fact influenced by a functional covariate process. We apply the spatial functional generalized linear model to a problem in which the objective is to relate COVID-19 vaccination rates in counties of states in the Midwestern United States to the number of new cases from previous weeks in those same geographic regions.

Keywords: spatial data, functional data analysis, generalized linear model

*Corresponding author
Email address: srkim@iastate.edu (Sooran Kim)

1. Introduction

In some problems we may have interest in a given spatially structured response at a single point in time, but believe that the response is influenced by some historical covariate process evolving over time at individual spatial locations. Examples of such problems can be drawn from meteorology, ecological and environmental sciences, and social sciences, in which some type of an event is influenced by environmental or behavioral conditions that develop over some prior time span. To deal with such situations, Kim et al. (2024) developed a class of one-parameter exponential family Markov random field models with a functional covariate regressor, which is a novel approach to associating a functional covariate process with spatially structured response variables. Due to the infinite-dimensionality of the regressor, the truncation strategy introduced in Müller and Stadtmüller (2005) was employed to handle the functional covariate. Simulation results in Kim et al. (2024) indicated that the use of composite likelihood estimation and Akaike information criterion (AIC) were promising for selecting the truncation level in these *spatial generalized functional linear* models (SGFLM).

Selecting the truncation level is crucial to model performance when the truncation strategy is applied to represent functional data. Common approaches include fraction of variance explained (FVE), AIC, and cross-validation (e.g., Goldsmith et al., 2011; Gertheiss et al., 2013; Müller and Stadtmüller, 2005; Jadhav et al., 2017). Under spatial dependence, selecting the truncation level remains important. Ahmed et al. (2022) introduced the functional spatial autoregressive model (FSAR) applying the truncation strategy. These authors compared the average squared error (ASE), AIC, and the Bayesian information criterion (BIC) to choose the truncation level, and found that the ASE and AIC outperform the other. In contrast, Kim et al. (2024) followed the truncation level selection criterion of Müller and Stadtmüller (2005) based on AIC, but did not explore other criteria for selecting the truncation level. In this article, we study methods to select the truncation level p in a SFGLM based on binary conditional response distributions.

In what follows, we consider five criteria to choose the truncation level: AIC based on the log composite likelihood, BIC based on the log composite likelihood, fraction of variance explained, fitted mean squared error, and cross-validated prediction error with one standard error rule. We compare simulation results using these criteria in Section 4 and find that BIC based on the log composite likelihood is the superior criterion, leading us to propose

a rule of thumb for choosing the truncation level.

We employ this rule of thumb in an analysis of COVID-19 data, in which the functional covariate is the number of new COVID cases over a period of time is related to the vaccination rate at the end of that time period. The question is whether there is evidence that the time course of disease prevalence is related to subsequent willingness to receive vaccination. A secondary question is whether the vaccine responses appear to be spatially structured beyond what might be produced by site-specific covariate processes. We demonstrate stability in the modeled relation by utilizing three different time periods over which the functional covariate is allowed to evolve. In addition, we find that spatial dependence in the new vaccination rate response is more pronounced in areas with higher populations than in areas with lower population levels, even after the covariate is accounted for.

The remainder of the article is organized as follows. Section 2 provides background information on the models and estimation methods proposed in Kim et al. (2024), as well as the asymptotic context in spatial statistics . We discuss different approaches to selecting the truncation level p in Section 3 and present numerical studies in Section 4. The aforementioned application to COVID vaccination rates is contained in Section 5. Concluding remarks are included in Section 6.

2. Background

2.1. Models

In this section we present the four models that will be used in the sequel. Let $\mathbf{s}_i = (u_i, v_i)$ denote a spatial location with horizontal coordinate u_i and vertical coordinate v_i in some appropriate coordinate system (e.g., universal transverse Mercator or latitude/longitude). Let $\{Y(\mathbf{s}_i)\}_{i=1}^n$ denote binary random variables associated with these spatial locations and having probability mass functions such that $Pr[Y(\mathbf{s}_i) = 1] = p(\mathbf{s}_i)$ and $Pr[Y(\mathbf{s}_i) = 0] = 1 - p(\mathbf{s}_i)$. Let $\{\mathbf{x}(\mathbf{s}_i)\}_{i=1}^n$ denote possibly vector valued spatially indexed covariates. In a Markov random field model, the probability $p(\mathbf{s}_i)$ is modeled as a function of the values of $\mathbf{x}(\mathbf{s}_i)$ and $\{Y(\mathbf{s}_j) : j \neq i\}$

as,

$$\begin{aligned} \log\left[\frac{p(\mathbf{s}_i)}{1-p(\mathbf{s}_i)}\right] &= \log\left[\frac{\kappa_i}{1-\kappa_i}\right] + \sum_{j\neq i}\eta_{i,j}\{y(\mathbf{s}_j)-\kappa_j\} \\ \log\left[\frac{\kappa_i}{1-\kappa_i}\right] &= g[\mathbf{x}(\mathbf{s}_i)], \end{aligned} \tag{1}$$

where $g(\cdot)$ is a known regression function. Typically, it is assumed that there exist defined neighborhoods of the spatial locations, denoted as $\{N_i\}_{i=1}^n$ such that $\eta_{i,j} = 0$ unless $\mathbf{s}_j \in N_i$. Classic examples of neighborhood structures on a regular lattice are four-nearest and eight-nearest specifications. There are also restrictions on the values of the dependence parameters $\eta_{i,j}$ needed for there to exist an identifiable joint distribution that contains the set of specified conditionals. Throughout this article we will assume $\eta_{i,j} = \eta$ for $\mathbf{s}_j \in N_i$. This condition is sufficient to allow a joint distribution to be identified through the use of the negpotential function of Besag (1974). (See Kaiser and Cressie (2000)). Model (1) constitutes a basic binary Markov random field model with spatially varying but fixed covariates. If $g(\cdot)$ is a linear combination of the components of $\mathbf{x}(\mathbf{s}_i)$ this model might be called a spatial generalized linear model (SGLM) with logit link. Note here, however, that it is the conditional, rather than marginal, mass functions of the response variables that are assigned a one-parameter exponential family form.

Now let X_i be a functional covariate at spatial location $\mathbf{s}_i$ that takes values in $\mathcal{L}_2(\mathcal{T})$, the set of all square-integrable functions on a closed interval $\mathcal{T}$. We assume that $EX_i = 0$ for $i = 1, \cdots, n$. To formulate a model with spatially indexed functional covariates we replace the last line of (1) with

$$\log\left[\frac{\kappa_i}{1-\kappa_i}\right] = \alpha + \int \beta(t)X_i(t)\,dt.$$

The truncation strategy of Müller and Stadtmüller (2005) is to approximate the previous integral by

$$g(X_i) = \alpha + \sum_{j=1}^{p}\beta_j \int X_i(t)\phi_j(t)dt, \tag{2}$$

where $\{\phi_j\}_{j=1}^{\infty}$ is a orthonormal basis and $\beta_j = \int \beta(t)\phi_j(t)\,dt$. Kim et al. (2024) referred to this as a *spatial generalized functional linear model* (SGFLM).

It is well known that in problems involving response variables that exhibit spatial structure there is no unique way to represent that structure in a model. Spatial patterns may be attributed to the effects of covariates or covariate processes and modeled through what is called the large-scale model component, which is represented in models for $\log[\kappa_i/(1-\kappa_i)]$ in (1) and (2). Alternatively, one may attribute spatial structure or pattern to internal processes that regulate response values and model that structure through what is called the small-scale model component, which is represented by the dependence parameter η in (1). This presents several other possibilities that might be considered in applications, and we include three of those possibilities here for the sake of comparison. First, one could take $\eta = 0$ in (1) combined with (2) which results in a *generalized functional linear model* (GFLM, Müller and Stadtmüller (2005)) without spatial dependency, having binary random component and logit link. Or, since temporal data are typically collected at discrete points in time, a covariate process could be aggregated over time to produce a single value at each location, and those values used as fixed covariates in the SGLM (1) with $\eta \neq 0$. For this, consider observations of the covariate process at discrete points in time so that at location $\mathbf{s}_i$ we observe $\{x_i(t)\}_{t=1}^{T}$, and define a fixed covariate value as the simple average of those values, $z(\mathbf{s}_i) = (1/T)\sum_t x_i(t)$ for $i = 1, \ldots, n$. Finally, one could also use an aggregated temporal covariate and also take $\eta = 0$, which would result in a traditional binary generalized linear model with logit link (GLM). Note that elaborations of each of these structures are possible by using more flexible structures than $\eta_{i,j} = \eta$ for the dependence parameters, and using regressions based on alternative link functions in (1). We consider four models based on cross combinations of two forms for the large scale component and two forms for the small scale component. Specifically, large scale model components were taken to be

$$\log\left(\frac{\kappa_i}{1-\kappa_i}\right) = \begin{cases} \alpha + \beta z(\mathbf{s}_i) & \text{for GLM, SGLM} \\ \alpha + \sum_{k=1}^{p} \beta_k \int X_i(t)\phi_k(t)dt & \text{for GFLM, SGFLM.} \end{cases} \tag{3}$$

Small scale model structures were taken as

$$\eta_{i,j} = \begin{cases} 0 \ \ \forall i, j & \text{for GLM, GFLM} \\ \eta \mathbb{I}(\mathbf{s}_j \in N_i) & \text{for SGLM, SGFLM,} \end{cases} \tag{4}$$

where $\mathbb{I}(A)$ is the indicator function that assumes a value of 1 if A is true and 0 otherwise.

Note that elaborations of each of the four model structures given in (3) and (4) are possible by using link functions other than the logit and using more flexible models for the dependence parameters.

2.2. Estimation

Two of the four models considered here make use of independent marginal binary distributions while two make use of conditionally specified binary distributions. Two contain a dependence parameter and two do not. It will be convenient to write these distributions in exponential family form and suppress explicit identification of conditioning quantities. A general representation for the probability mass function of response variables $\{Y(\mathbf{s}_i)\}_{i=1}^n$ is then,

$$f(y(\mathbf{s}_i)|\cdot) = \exp\left[A_i y(\mathbf{s}_i) - B(A_i)\right]. \tag{5}$$

In each of the models we have

$$B(A_i) = \log[1 + \exp(A_i)],$$

and

$$E[Y(\mathbf{s}_i)|\cdot] = \frac{\exp(A_i)}{1 + \exp(A_i)}.$$

The models we consider may then be distinguished based on additional modeling of the function A_i. Let θ represent generic notation for whatever specific parameters are required in this additional modeling. For the GLM and GFLM models,

$$A_i = \log\left(\frac{\kappa_i}{1 - \kappa_i}\right), \tag{6}$$

so that the A_i are given directly and completely in (3) where $\theta = (\alpha, \beta)^\top$ for GLM and $\theta = (\alpha, \beta_1, \ldots, \beta_p)^\top$ for GFLM. For the SGLM and SGFLM models, the A_i are given as

$$A_i = \log\left(\frac{\kappa_i}{1 - \kappa_i}\right) + \eta \sum_{\mathbf{s}_j \in N_i} \{y(\mathbf{s}_j) - \kappa_j\} \tag{7}$$

where $\theta = (\eta, \alpha, \beta)^\top$ for SGLM and $\theta = (\eta, \alpha, \beta_1, \ldots, \beta_p)^\top$ for SGFLM.

It is worth noting at this point that the conditioning sets for response probability mass functions (5) differ among the models considered. For the GLM model this set includes only fixed covariates $\{z(\mathbf{s}_i)\}_{i=1}^n$ and $\theta = (\alpha, \beta)^\top$.

For the SGLM model the conditioning set contains fixed covariates $\{z(\mathbf{s}_i)\}_{i=1}^n$, neighboring values $\mathbf{y}(N_i) = \{y(\mathbf{s}_j) : j \in N_i\}$ and $\theta = (\eta, \alpha, \beta)^\top$. Response distributions for the GFLM are conditioned on $\{X_i\}_{i=1}^n$ and $\theta = (\alpha, \beta_1, \ldots, \beta_p)^\top$, while those for the SGFLM are conditioned on $\{X_i\}_{i=1}^n$, $\mathbf{y}(N_i) = \{y(\mathbf{s}_j) : j \in N_i\}$, and $\theta = (\eta, \alpha, \beta_1, \ldots, \beta_p)^\top$.

Estimation can be based on maximization of the objective function,

$$Q = \sum_{i=1}^{n} \log\{f(y(\mathbf{s}_i)|\cdot)\}. \tag{8}$$

For GLM and GFLM, (8) is a likelihood, and its maximization results in simultaneous maximum likelihood estimates of the elements in θ. For SGLM and SGFLM, (8) is a composite likeihood and its maximization results in maximum composite likelihood estimates. Note that for the SGLM, (8) corresponds to the original pseudo-likelihood of Besag (1975). For comparison, we also included quasi-likelihood estimates for the GFLM as suggested by Müller and Stadtmüller (2005).

In the case of the GFLM and SGFLM, the estimated function parameter $\hat{\beta}(t)$ can be obtained as

$$\hat{\beta}(t) = \sum_{j=1}^{p} \hat{\beta}_j \phi_j(t).$$

2.3. Inference

With a functional covariate in the GFLM and SGFLM, the primary target of inference is the regression process $\beta(t)$, with the addition of η for the SGFLM. In these two models we also have the possibility of making inferential statements about the intercept parameter α and the parameters in the truncated regression $\beta_1, \ldots, \beta_p$. In the results to follow we focus on confidence bands for $\beta(t)$ and coverage of confidence intervals for η.

Müller and Stadtmüller (2005) give results that lead to inferential quantities for the GFLM under quasi-likelihood estimation. In the usual independent and identically distributed case, we assume that the truncation level $p = p_n$ diverges as the sample size n diverges. On the other hand, for spatial models on discrete lattice systems there can be several asymptotic contexts, often referred to as repeating lattice and expanding lattice contexts (e.g., Varin and Firth (2011)). In the repeating lattice asymptotic context, N independent realizations on a given fixed finite location were observed, and the

number of independent realizations N tends to infinity. We also assume that the truncation level $p = p_N$ diverges as the number of independent copies N goes to infinity. Kim et al. (2024) develop asymptotic results for the SGFLM that can be used to compute confidence bands in this context. Asymptotic results are most easily developed under the repeating lattice context and typically result in the use of inverse Godambe information to compute inferential quantities, as in Kim et al. (2024). For many applications, however, the expanding lattice context is more easily conceptualized. In the expanding lattice context, we assume that the spatial locations expand without bound, and the truncation level $p = p_n$ diverges as the spatial locations n expands. Under strong mixing conditions the results for repeating lattices hold here as well (Guyon (1995)), although without replication estimation of Godambe information can become more difficult.

In what follows, we rely on asymptotic normality of maximum likelihood, maximum quasi-likelihood and maximum composite likelihood estimators in forming confidence intervals for η and pointwise confidence bands for $\beta(t)$. Comparison of estimators when applied to data generated from the SGFLM in Section 4 will be based on Monte Carlo approximations to quantities such as mean squared errors. Before presenting simulation results on the comparison of estimators, however, we turn our attention to selection of the truncation level p in (2) which impacts all aspects of estimaton and inference.

3. Selection of the Truncation Level

The process of selecting the truncation level in a functional model is significant because the estimation results can vary depending on the chosen truncation level. To address this issue, we use five criteria to choose the truncation level p: AIC based on the log composite likelihood (AIC_c), BIC based on the log composite likelihood (BIC_c), fraction of variance explained (FVE), fitted mean squared error (FMSE), and prediction error with one standard error rule (PE with 1se rule).

Let k be the number of parameters in the model and $\hat{l}$ be the maximized value of the log likelihood. The AIC is defined as $\text{AIC} = 2k - 2\hat{l}$. However, in a spatial model, it is often difficult to compute the maximum likelihood because the density of the model is given as an intractable form. We can use the log composite likelihood instead of the log likelihood. Let $\hat{l}_c$ be the maximized value of the log composite likelihood. The AIC_c can be defined

as

$$\mathrm{AIC_c} = 2k - 2\hat{l}_c.$$

We choose the truncation level when the $\mathrm{AIC_c}$ has the minimum value in the same way as the AIC. Although the AIC is the most popular criterion for model selection, it tends to favor high dimension models.

Let n be the number of observations. The BIC, an alternative tool of the AIC, is defined as $\mathrm{BIC} = kln(n) - 2\hat{l}$. Similar to $\mathrm{AIC_c}$, the $\mathrm{BIC_c}$ can be defined as

$$\mathrm{BIC_c} = klog(n) - 2\hat{l}_c.$$

We select the truncation level having the smallest value of $\mathrm{BIC_c}$ in the same way as the BIC. Compared to the AIC, the penalty for additional parameters is greater in the BIC, which means that the BIC tends to choose more parsimonious models than does AIC.

FVE by the first M functional principal components is a measure of how much of the total variance in the data is explained by the first M principal components. It is defined as the ratio between the sum of the variances of the first M principal components and the sum of the variances of all principal components. Mathematically, this can be expressed as

$$\mathrm{FVE}(M) = \frac{\sum_{m=1}^{M} \lambda_m}{\sum_{m=1}^{\infty} \lambda_m}$$

where λ_m is the mth eigenvalue of the covariance function G defined as $G(s,t) = cov(X(t), X(s))$ for $t, s \in \mathcal{T}$. Using the FVE criterion, the truncation level is selected as the smallest value of M such that $\mathrm{FVE}(M) \geq \gamma$, where γ is a pre-specified threshold value between 0 and 1. This criterion is commonly used in functional data analysis to select the number of functional principal components to retain, as it provides a way to balance model complexity and the amount of explained variability in the data. However, it is important to note that this criterion only considers the functional covariate and may not take into account other relevant factors that could affect the model selection process.

FMSE is a measure of the average squared difference between the observed and the estimated conditional expected value. Specifically, it is defined as

$$\mathrm{FMSE} = \frac{1}{n} \sum_{i=1}^{n} (y(\mathbf{s}_i) - \hat{p}(\mathbf{s}_i))^2,$$

where

$$\hat{p}(\mathbf{s}_i) = \frac{\exp(\hat{A}_i)}{1 + \exp(\hat{A}_i)}.$$

For the GFLM, $\hat{A}_i$ can be obtained from (6) using estimated parameters $(\hat{\alpha}, \hat{\beta}_1, \ldots, \hat{\beta}_p)^\top$, while for SGFLM, $\hat{A}_i$ can be obtained from (7) using estimated parameters $(\hat{\eta}, \hat{\alpha}, \hat{\beta}_1, \ldots, \hat{\beta}_p)^\top$. To select the truncation level using FMSE, we can choose the truncation level that minimizes the FMSE. However, as the truncation level increases, FMSE usually tends to decrease, which may lead to choosing a larger truncation level than necessary. To address this issue, we can consider the change of FMSE as the truncation level increases. Specifically, we choose the truncation level that maximizes the change of FMSE. If FMSE is a non-decreasing function of the truncation level, then we can simply choose the truncation level that minimizes the FMSE. This criterion can help avoid overfitting the model and achieve dimension reduction.

PE with 1se rule is a method used for selecting the truncation level in functional data analysis. First, the prediction error can be obtained from the following step. (a) Randomly select one observation and choose a non-overlapping neighbor as a leave-out point. (b) Repeat step (a) until 5% of the total observations are selected as test data, ensuring that each observation in the training data has at least three neighbors. (c) Estimate the model parameters for each truncation level using the training data and predict the response variable for the test data. The prediction is obtained by assigning 1 to observations with $\hat{p}(\mathbf{s}_i) > 0.5$ and 0 to observations with $\hat{p}(\mathbf{s}_i) \leq 0.5$. (d) Compute the prediction error for each truncation level. (e) Repeat steps (a) to (d) 20 times. (f) Calculate the average prediction error for each truncation level. After obtaining the prediction error, the one standard error rule is applied. The minimum prediction error among the truncation levels is identified, and the simplest model whose average prediction error falls within one standard deviation of the minimum prediction error is selected. This method can help avoid overfitting and select a simpler model, but it can be computationally expensive.

4. Simulation

4.1. Simulation design

We employed a simulation design similar to Kim et al. (2024). Random samples $\{X_i, Y(\mathbf{s}_i)\}_{i=1}^n$ following SGFLM were generated on a regular lat-

tice wrapped on a torus with a four-nearest neighborhood structure. Three sample sizes $n = 400, 900, 1600$, on the regular lattice 20×20, 30×30, or 40×40 respectively, were considered in the following results. The functional covariate was evaluated at 50 equally spaced points ranging from 0 to 1, and generated as $X_i(t) = \mu(t) + \sum_{j=1}^{20} \varepsilon_j^{(i)} \phi_j(t)$ where $\mu(t) = 4t \sin(3t)$, $\varepsilon_j^{(i)}$ follows a normal distribution with mean 0 and variance $1/j^2$, and $\{\phi_j(t)\}_{j=1}^{\infty}$ denotes the first 20 functions from the trigonometric base. We set $\alpha = 0$ and defined $\beta(t) = \sum_{j=1}^{20} \beta_j \phi_j(t)$, where $\beta_j = j^{-1}$ for $j = 1, 2, 3$ and 0 for $j > 3$. The parameter function $\beta(t)$ was also evaluated at 50 equally spaced points ranging from 0 to 1. The response variables were generated through a Gibbs Sampling algorithm. Initial values were drawn from independent Bernoulli distributions with a probability of 0.5. Then the $200th$ data set was used as a response. Finally, $M = 1000$ Monte Carlo simulations were obtained.

4.2. Assessment criteria

Monte Carlo approximations to the expected values of η and α were computed. For example, for η,

$$\mathrm{E}_M(\hat{\eta}) = \frac{1}{M} \sum_{m=1}^{M} \hat{\eta}_m,$$

and similarly for α. Mean squared error (MSE) for scalar parameters and mean integrated squared error (MISE) for a parameter function were used as measures of total error in estimation. For example, MSE for the scalar estimator η and MISE for the parameter function $\beta(t)$ were defined as

$$\mathrm{MSE}_M(\hat{\eta}) = \frac{1}{M} \sum_{m=1}^{M} (\eta - \hat{\eta}_m)^2, \quad \mathrm{MISE}_M(\hat{\beta}) = \frac{1}{M} \sum_{m=1}^{M} \int (\beta(t) - \hat{\beta}_m(t))^2 dt$$

respectively. Also, we computed a Monte Carlo approximation to $\int var(\hat{\beta}(t))$ as

$$\mathrm{IV}_M(\hat{\beta}) = \frac{1}{M} \sum_{m=1}^{M} \int (\hat{\beta}_m(t) - E[\hat{\beta}_m(t)])^2 dt.$$

The empirical coverage of 95% confidence interval for η was calculated by

$$\mathrm{CI}_M = \frac{1}{M} \sum_{m=1}^{M} \mathbb{I}(\eta \in CI_m)$$

where $\mathbb{I}$ is the indicator function. Finally, the average of FMSE defined in Section 3, is also used to compare models in the following subsections.

4.3. Selection of truncation level p

In this subsection, we study a comprehensive examination involving selecting the truncation level p based on five criteria, as described in Section 3. This analysis encompasses the evaluation of estimation results and inferences contingent upon the chosen truncation level p and suggests our rule of thumb to select the truncation level p. We first use $\mathrm{AIC_c}$, akin to the methodology employed in Müller and Stadtmüller (2005). Figure 1 presents the histograms of p chosen by $\mathrm{AIC_c}$. Notably, $\mathrm{AIC_c}$ tends to favor larger values of the truncation level as the spatial parameter η increases, but it converges towards the true truncation level $p = 3$ as the sample size n increases. Compared to Figure 1, the histograms of p selected by $\mathrm{BIC_c}$ in Figure 2 are more concentrated on smaller values of truncation level p. The choice of truncation level via $\mathrm{BIC_c}$ remains relatively unaffected by variations in the spatial parameter η, however, it leans towards $p = 2$ or 3 as the sample size n increases. Moving on to the third criterion FVE, Figure 3 illustrates the histograms of p selected by FVE. FVE frequently selects one or two values for the truncation level p. For example, the truncation level p is selected as 4 or 5 when using the FVE exceeding 90%. Furthermore, to account for more than 90% of the data variance, FVE tends to favor relatively larger values of truncation level p. Figure 4 displays the histograms of the selected truncation level p based on the big change of FMSE. For smaller sample sizes, specifically $n = 400$, relatively larger values of p are preferred. Although it still selects some large values of truncation level p with large sample sizes, such as $n = 1600$, there is a tendency for smaller values of p to be chosen more frequently as the sample size n increases. Lastly, PE with 1se rule shows the behavior between $\mathrm{AIC_c}$ and $\mathrm{BIC_c}$ in Figure 5. PE with 1se rule tends to select smaller values of truncation level p in comparison to $\mathrm{AIC_c}$, while selecting larger values of truncation level p when contrasted with $\mathrm{BIC_c}$.

These aspects impact the estimation results in Table 1-2. Through Table 1-2, the accuracy and precision in estimation of the spatial parameter η was quite good for all five criteria regardless of the sample size n. For all five criteria, MISE for the parameter function $\beta(t)$ decreases as the sample size n increases. Notably, MISE for the parameter function $\beta(t)$ is relatively big when the truncation level p is selected by $\mathrm{AIC_c}$ or the big change of FMSE for the small sample size $n = 400$. This is primarily because they tends to select larger values of truncation level p. On the other hand, $\mathrm{BIC_c}$ consistently yields the smallest MISE values for the parameter function $\beta(t)$ across a spectrum of spatial parameter η and sample size n. Coverage of

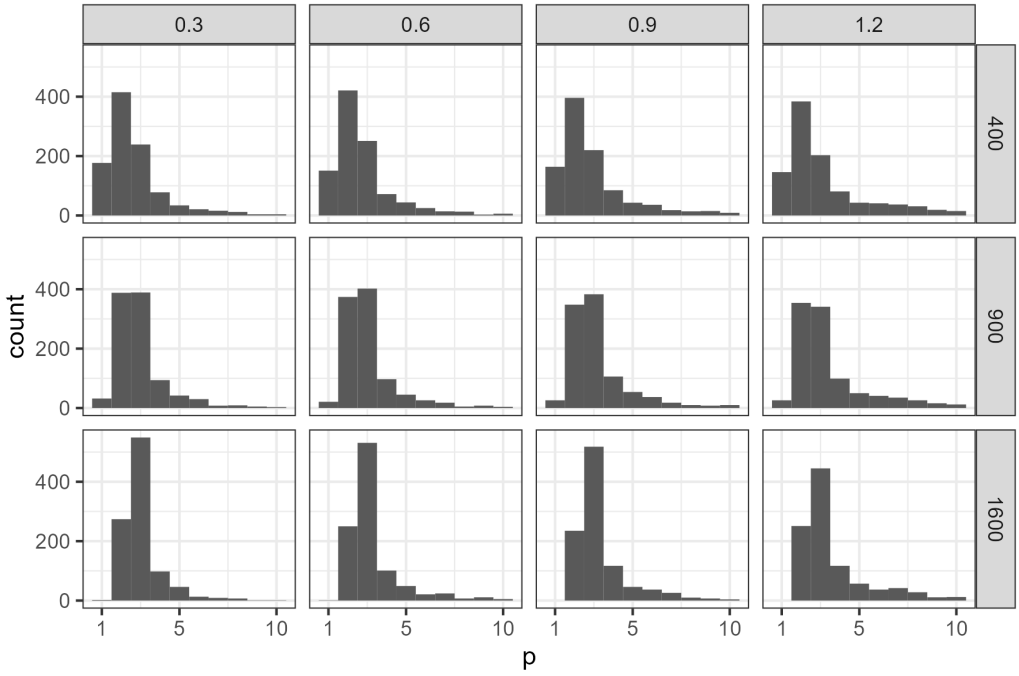

Figure 1: (Histogram of p selected by $\mathrm{AIC_c}$) The columns represent the spatial parameter η and the rows represent the sample size n

confidence intervals for the spatial dependence parameter η, improves as the spatial parameter η increases, and this holds for all five criteria. Figure 6-7 display the confidence bands for $\beta(t)$ based on the truncation level selected by $\mathrm{AIC_c}$ and $\mathrm{BIC_c}$, respectively. These bands tend to widen as the spatial parameter η increases and narrow as the sample size n grows in both figures. When the truncation level p is selected by $\mathrm{AIC_c}$, the confidence bands for $\beta(t)$ are wider than those generated by $\mathrm{BIC_c}$. For the other three criteria, namely FVE (90%), the big change of FMSE, and PE with 1se rule, we can see the same behavior. Therefore, we propose a rule of thumb for selecting the truncation level p as $\mathrm{BIC_c}$.

4.4. Model comparison

In this subsection, we demonstrate the superior performance of SGFLM in comparison to other models. First, we compare the four models described in Section 2 by FMSE, before the truncation level is selected. Figure 8 illustrates the FMSE values of four models for various truncation levels, denoted

		AIC_c				BIC_c			
$n = 400$	$E_M(\hat{\eta})$	0.30	0.61	0.94	1.27	0.29	0.60	0.91	1.24
	$MSE_M(\hat{\eta})$	0.05	0.04	0.04	0.04	0.04	0.04	0.04	0.03
	$E_M(\hat{\alpha})$	-0.08	-0.05	-0.08	-0.40	-0.30	-0.27	-0.27	-0.58
	$MSE_M(\hat{\alpha})$	0.13	0.15	0.27	0.91	0.22	0.21	0.30	1.06
	$MISE_M(\hat{\beta})$	0.88	0.97	1.33	1.89	0.35	0.35	0.35	0.37
	$IV_M(\hat{\beta}(t))$	0.87	0.96	1.32	1.88	0.22	0.23	0.23	0.26
	$CI_M(\eta)$	0.83	0.86	0.83	0.85	0.82	0.86	0.85	0.89
$n = 900$	$E_M(\hat{\eta})$	0.30	0.61	0.92	1.22	0.30	0.61	0.91	1.21
	$MSE_M(\hat{\eta})$	0.02	0.02	0.02	0.01	0.02	0.02	0.02	0.01
	$E_M(\hat{\alpha})$	-0.03	-0.02	-0.03	-0.25	-0.19	-0.18	-0.18	-0.37
	$MSE_M(\hat{\alpha})$	0.06	0.06	0.10	0.47	0.10	0.11	0.15	0.55
	$MISE_M(\hat{\beta})$	0.37	0.42	0.54	0.73	0.21	0.22	0.22	0.23
	$IV_M(\hat{\beta}(t))$	0.36	0.42	0.54	0.73	0.14	0.14	0.15	0.17
	$CI_M(\eta)$	0.84	0.86	0.86	0.89	0.84	0.85	0.86	0.90
$n = 1600$	$E_M(\hat{\eta})$	0.30	0.61	0.91	1.21	0.30	0.60	0.90	1.21
	$MSE_M(\hat{\eta})$	0.01	0.01	0.01	0.01	0.01	0.01	0.01	0.01
	$E_M(\hat{\alpha})$	-0.03	-0.01	-0.02	-0.13	-0.12	-0.12	-0.12	-0.22
	$MSE_M(\hat{\alpha})$	0.03	0.04	0.04	0.23	0.05	0.06	0.07	0.27
	$MISE_M(\hat{\beta})$	0.17	0.26	0.26	0.37	0.13	0.14	0.14	0.15
	$IV_M(\hat{\beta}(t))$	0.17	0.26	0.26	0.37	0.09	0.10	0.11	0.11
	$CI_M(\eta)$	0.83	0.85	0.87	0.89	0.84	0.85	0.87	0.89

Table 1: Estimation of parameters with the sample size $n \in \{400, 900, 1600\}$ and the spatial dependence parameter $\eta \in \{0.3, 0.6, 0.9, 1.2\}$ depending on AIC_c and BIC_c

		FVE (90%)				FMSE				PE with 1se rule			
$n = 400$	$\mathrm{E}_M(\hat{\eta})$	0.30	0.62	0.95	1.27	0.30	0.62	0.95	1.27	0.30	0.59	0.91	1.22
	$\mathrm{MSE}_M(\hat{\eta})$	0.05	0.04	0.04	0.03	0.05	0.04	0.04	0.03	0.04	0.04	0.04	0.03
	$\mathrm{E}_M(\hat{\alpha})$	-0.01	0.03	-0.01	-0.34	-0.08	-0.06	-0.09	-0.44	-0.37	-0.32	-0.35	-0.60
	$\mathrm{MSE}_M(\hat{\alpha})$	0.11	0.13	0.25	0.88	0.09	0.11	0.24	0.96	0.22	0.23	0.37	1.05
	$\mathrm{MISE}_M(\hat{\beta})$	0.83	0.85	0.95	0.97	1.87	2.00	2.44	2.44	0.35	0.57	0.53	0.52
	$\mathrm{IV}_M(\hat{\beta}(t))$	0.82	0.85	0.94	0.96	1.85	1.97	2.42	2.41	0.16	0.41	0.36	0.34
	$\mathrm{CI}_M(\eta)$	0.84	0.87	0.85	0.87	0.83	0.86	0.84	0.87	0.84	0.83	0.82	0.90
$n = 900$	$\mathrm{E}_M(\hat{\eta})$	0.30	0.62	0.92	1.22	0.30	0.61	0.91	1.21	0.29	0.60	0.89	1.19
	$\mathrm{MSE}_M(\hat{\eta})$	0.02	0.02	0.02	0.01	0.02	0.02	0.02	0.01	0.02	0.02	0.02	0.01
	$\mathrm{E}_M(\hat{\alpha})$	-0.00	0.01	0.00	-0.20	-0.13	-0.11	-0.12	-0.33	-0.34	-0.32	-0.33	-0.52
	$\mathrm{MSE}_M(\hat{\alpha})$	0.05	0.06	0.10	0.43	0.05	0.05	0.09	0.49	0.18	0.18	0.21	0.68
	$\mathrm{MISE}_M(\hat{\beta})$	0.36	0.39	0.41	0.43	0.40	0.46	0.49	0.55	0.34	0.34	0.32	0.34
	$\mathrm{IV}_M(\hat{\beta}(t))$	0.36	0.39	0.41	0.43	0.34	0.40	0.44	0.50	0.16	0.17	0.15	0.19
	$\mathrm{CI}_M(\eta)$	0.84	0.86	0.86	0.90	0.84	0.85	0.86	0.90	0.83	0.83	0.86	0.89
$n = 1600$	$\mathrm{E}_M(\hat{\eta})$	0.30	0.61	0.91	1.21	0.29	0.60	0.90	1.20	0.30	0.59	0.89	1.19
	$\mathrm{MSE}_M(\hat{\eta})$	0.01	0.01	0.01	0.01	0.01	0.01	0.01	0.01	0.01	0.01	0.01	0.01
	$\mathrm{E}_M(\hat{\alpha})$	-0.00	0.01	0.00	-0.11	-0.16	-0.15	-0.15	-0.26	-0.32	-0.31	-0.33	-0.43
	$\mathrm{MSE}_M(\hat{\alpha})$	0.03	0.03	0.04	0.23	0.04	0.04	0.06	0.27	0.16	0.15	0.17	0.41
	$\mathrm{MISE}_M(\hat{\beta})$	0.20	0.21	0.22	0.24	0.16	0.17	0.18	0.19	0.27	0.28	0.29	0.29
	$\mathrm{IV}_M(\hat{\beta}(t))$	0.20	0.21	0.22	0.24	0.08	0.09	0.10	0.11	0.11	0.12	0.12	0.11
	$\mathrm{CI}_M(\eta)$	0.84	0.85	0.86	0.88	0.84	0.85	0.87	0.89	0.84	0.84	0.85	0.90

Table 2: Estimation of parameters with the sample size $n \in \{400, 900, 1600\}$ and the spatial dependence parameter $\eta \in \{0.3, 0.6, 0.9, 1.2\}$ depending on FVE (90%), the big change of FMSE, and PE with 1se rule

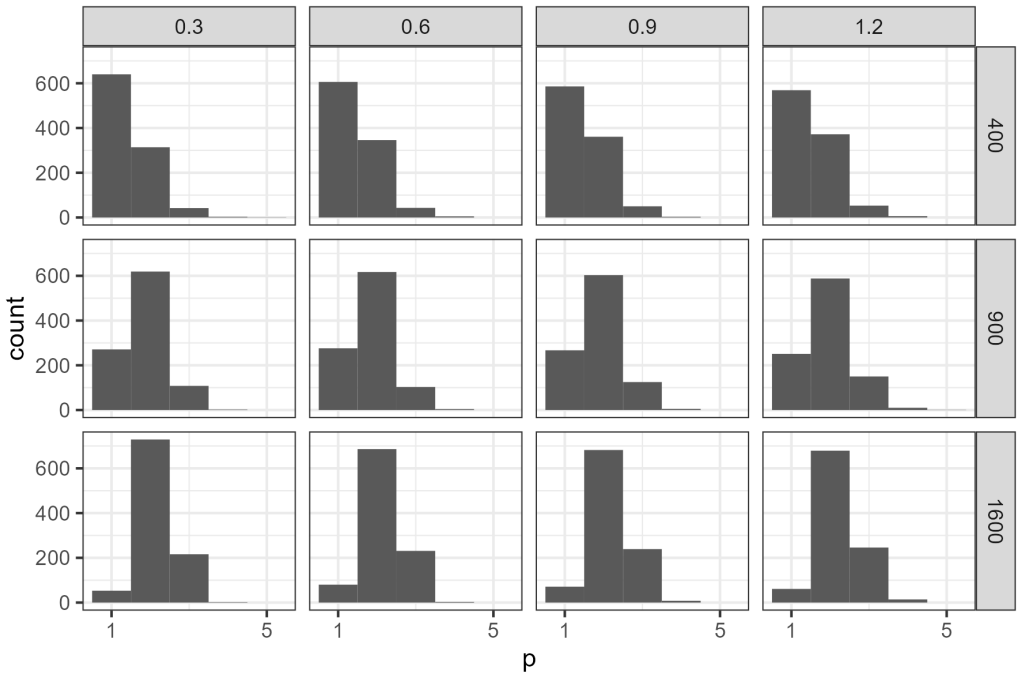

Figure 2: (Histogram of p selected by $\mathrm{BIC_c}$) The columns represent the spatial parameter η and the rows represent the sample size n

as $p = 1, \cdots, 10$. It is worth noting that GLM and SGLM do not necessitate the selection of the truncation level p. Therefore, we use the FMSE value for $p = 1$ as a representative for $p = 2, \cdots, 10$. First of all, we observe that spatial models, specifically SGLM and SGFLM, consistently exhibit smaller FMSE compared to independent models, GLM and GFLM, except when there is small spatial dependence with $\eta = 0.3$. As the spatial parameter η increases, the differences in FMSE between spatial and independent models increase. Furthermore, as the sample size n grows, the distinctions among independent models, as well as between spatial models, become less pronounced. Across all truncation levels ($p = 1, \cdots, 10$), however, SGFLM consistently outperforms other models in terms of FMSE, regardless of the spatial parameter η and the sample size n. Additionally, for sufficiently large sample sizes, for example, $n = 900$ or $n = 1600$, both GFLM and SGFLM have lower FMSE values when compared to GLM and SGLM, respectively. Given that GLM and SGLM do not require the selection of the truncation level p, we will focus exclusively on GFLM and SGFLM for the further model

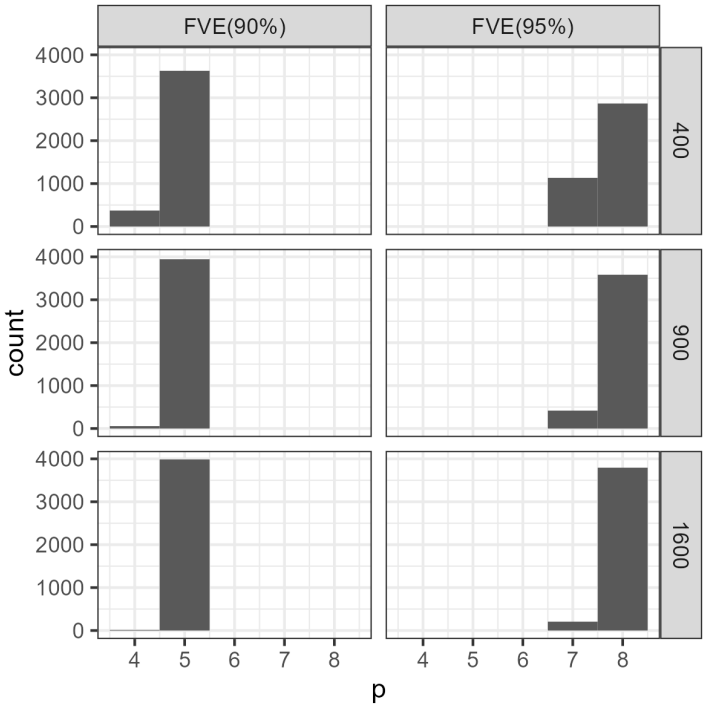

Figure 3: (Histogram of p selected by FVE) The columns represent the spatial parameter η and the rows represent the sample size n

comparison based on our rule of thumb.

We perform the same procedure for GFLM, although the results are not included here. As a result, we have determined that BIC is our preferred strategy for selecting the truncation level in GFLM, among the five criteria discussed in Section 3. Thus, we proceed to compare the estimation results and inference of GFLM and SGFLM using the truncation level p selected by BIC and BIC_c, respectively. In Table 3, we observe that MSE for α and MISE for $\beta(t)$ decrease as the sample size n increases for both models. Additionally, we notice that MISE for $\beta(t)$ increases as the spatial parameter η increases for both models. SGFLM stands out with the smallest value of MISE for $\beta(t)$ and the lowest value of FMSE. Figure 9 displays the confidence band of $\beta(t)$ of GFLM. Unlike Figure 7, the true function is not included in the confidence band for all cases. Consequently, we assert that SGFLM exhibits superiority over other models, based on FMSE.

		GFLM (Quasi)				GFLM (MLE)				SGFLM			
	η	0.3	0.6	0.9	1.2	0.3	0.6	0.9	1.2	0.3	0.6	0.9	1.2
$n = 400$	$\mathrm{E}_M(\hat{\eta})$	-	-	-	-	-	-	-	-	0.288	0.596	0.915	1.241
	$\mathrm{MSE}_M(\hat{\eta})$	-	-	-	-	-	-	-	-	0.044	0.038	0.037	0.030
	$\mathrm{E}_M(\hat{\alpha})$	0.034	-0.004	-0.162	-0.591	-0.309	-0.301	-0.379	-0.721	-0.303	-0.273	-0.268	-0.581
	$\mathrm{MSE}_M(\hat{\alpha})$	0.092	0.104	0.124	0.449	0.210	0.206	0.252	0.640	0.217	0.213	0.299	1.060
	$\mathrm{MISE}_M(\hat{\beta})$	0.432	0.446	0.435	0.439	0.344	0.347	0.362	0.403	0.351	0.354	0.347	0.369
	$\mathrm{IV}_M(\hat{\beta}(t))$	0.165	0.166	0.131	0.100	0.199	0.200	0.170	0.127	0.215	0.229	0.233	0.261
	$\mathrm{CI}_M(\eta)$	-	-	-	-	-	-	-	-	0.821	0.858	0.850	0.893
	FMSE	0.186	0.186	0.186	0.186	0.183	0.187	0.197	0.217	0.179	0.176	0.171	0.161
$n = 900$	$\mathrm{E}_M(\hat{\eta})$	-	-	-	-	-	-	-	-	0.296	0.607	0.905	1.207
	$\mathrm{MSE}_M(\hat{\eta})$	-	-	-	-	-	-	-	-	0.017	0.016	0.015	0.012
	$\mathrm{E}_M(\hat{\alpha})$	0.107	0.063	-0.105	-0.545	-0.192	-0.217	-0.300	-0.666	-0.186	-0.178	-0.178	-0.366
	$\mathrm{MSE}_M(\hat{\alpha})$	0.063	0.055	0.073	0.348	0.104	0.113	0.162	0.505	0.101	0.109	0.147	0.554
	$\mathrm{MISE}_M(\hat{\beta})$	0.348	0.344	0.323	0.362	0.213	0.222	0.239	0.321	0.212	0.217	0.218	0.226
	$\mathrm{IV}_M(\hat{\beta}(t))$	0.147	0.132	0.093	0.069	0.138	0.126	0.115	0.087	0.141	0.144	0.154	0.173
	$\mathrm{CI}_M(\eta)$	-	-	-	-	-	-	-	-	0.837	0.852	0.860	0.899
	FMSE	0.185	0.185	0.185	0.185	0.182	0.187	0.197	0.218	0.180	0.176	0.171	0.163
$n = 1600$	$\mathrm{E}_M(\hat{\eta})$	-	-	-	-	-	-	-	-	0.295	0.602	0.900	1.207
	$\mathrm{MSE}_M(\hat{\eta})$	-	-	-	-	-	-	-	-	0.009	0.009	0.008	0.007
	$\mathrm{E}_M(\hat{\alpha})$	0.144	0.092	-0.063	-0.480	-0.132	-0.155	-0.237	-0.593	-0.124	-0.115	-0.115	-0.223
	$\mathrm{MSE}_M(\hat{\alpha})$	0.048	0.040	0.038	0.266	0.054	0.063	0.094	0.394	0.051	0.058	0.067	0.273
	$\mathrm{MISE}_M(\hat{\beta})$	0.288	0.296	0.266	0.288	0.136	0.147	0.170	0.246	0.133	0.140	0.144	0.145
	$\mathrm{IV}_M(\hat{\beta}(t))$	0.125	0.114	0.064	0.053	0.085	0.086	0.079	0.067	0.087	0.099	0.105	0.110
	$\mathrm{CI}_M(\eta)$	-	-	-	-	-	-	-	-	0.836	0.849	0.867	0.891
	FMSE	0.185	0.185	0.185	0.185	0.183	0.187	0.198	0.219	0.180	0.176	0.172	0.163

Table 3: Estimation of parameters based on the truncation level selected by $\mathrm{BIC_c}$ with the spatial parameter $\eta \in \{0.3, 0.6, 0.9, 1.2\}$ and the sample size $n \in \{400, 900, 1600\}$

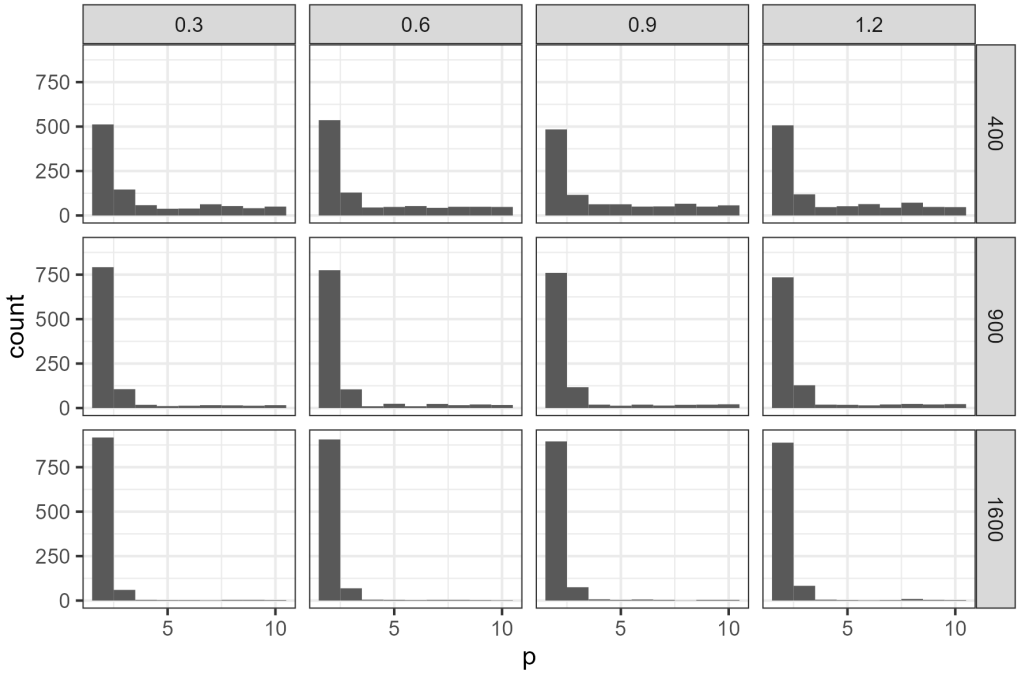

Figure 4: (Histogram of p selected by the big change of FMSE) The columns represent the spatial parameter η and the rows represent the sample size n

5. Application: COVID19

5.1. Data Description

In December 2019, a viral infection called coronavirus disease 2019 (COVID-19) was discovered in Wuhan, Hubei Province, China. COVID-19 is a contagious disease caused by the SARS-CoV-2 virus. It is highly infectious and has spread worldwide quickly. World Health Organization (WHO) declared a pandemic on March 11. COVID-19 can spread through droplets and very small particles containing the virus. People can be infected by many routes such as other infected people or contaminated surfaces they touch. Even if infected people do not have any symptoms, they can spread the virus. In 2020, two mRNA COVID-19 vaccines, the Pfizer-BioNTech and the Moderna COVID-19 vaccines, got authorization from FDA, and COVID-19 vaccines have been given to the public since December 2020.

In this paper, we are interested in the relationship between vaccination and the new infection case. We analyzed the relationship based on the 1054

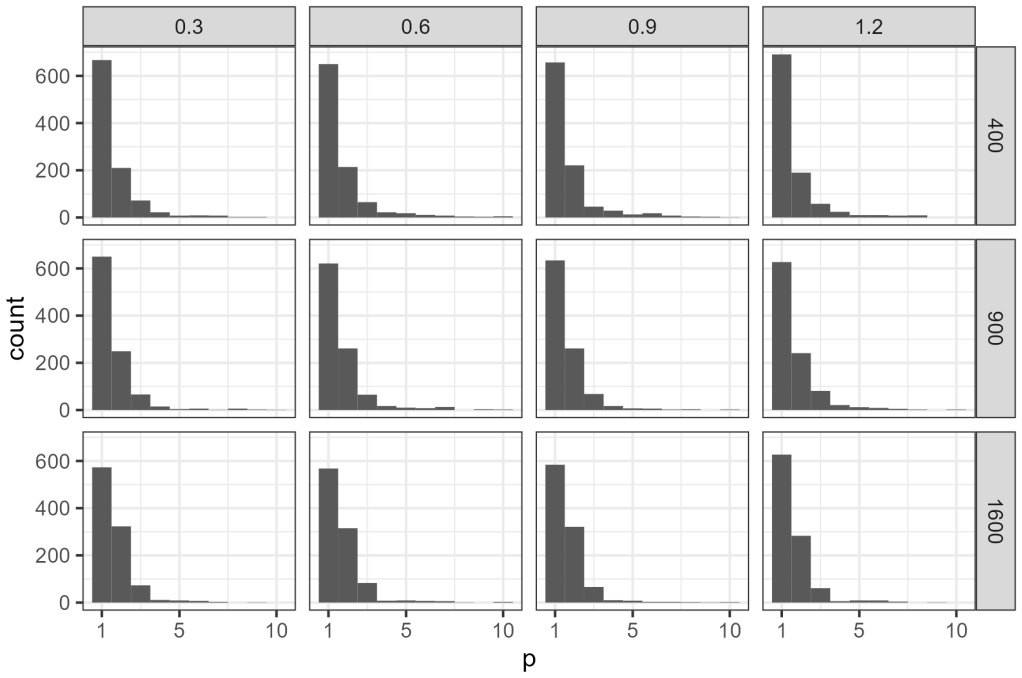

Figure 5: (Histogram of p selected by PE with 1se rule) The columns represent the spatial parameter η and the rows represent the sample size n

counties in the Midwestern United States. We obtained three types of data. The first data is the number of positive cases from the New York Times GitHub. It should be cumulative data, however, the number of positive cases declines in some cases. This can happen when a county corrects an error in the number of positive cases they have reported in the past, or when a state moves cases from one county to another. To correct this, we used the pool adjacent violators algorithm through `pava` function in `Iso` package in `R`. The second type of data obtained were the total number of people who are fully vaccinated from the Centers for Disease Control and Prevention (CDC). Being fully vaccinated means that one has finished the second dose of a two-dose vaccine or one dose of a single-dose vaccine. Finally, we also obtained the total population from Census Bureau. It was used in computation of the functional covariate and the response variables described presently.

All data were recorded daily. The daily data were transformed into the weekly values. For example, the daily number of positive cases data from January 10, 2021 to May 29, 2021 was transformed into the 20 weeks data

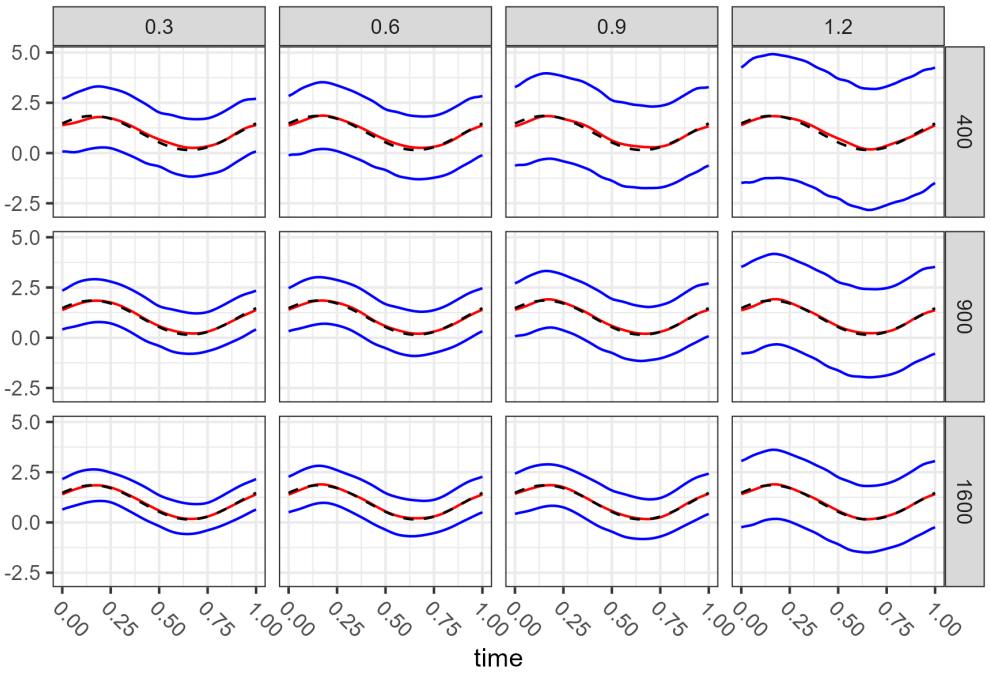

Figure 6: Confidence band of $\beta(t)$ based on the truncation level p selected by $\mathrm{AIC_c}$. The columns represent the spatial parameter η and the rows represent the sample size n. The dotted black line is the true $\beta(t)$, the red line is the average of $\hat{\beta}(t)$, and the blue lines are the average of confidence bands of $\beta(t)$

as the average during the week. As the functional covariate, we defined the new infection rate (%) over the week as

$$\frac{\text{(mean of the number of new positive cases during the week)}}{\text{susceptible population}} \times 100(\%).$$

where the susceptible population is defined as the population excluding the cumulative number of fully vaccinated people and positive cases until last week. It assumed that fully vaccinated people or already infected people are not infected easily. On the other hand, the new vaccination rate (%) over the week is defined as

$$\frac{\text{(mean of the number of fully vaccinated people during the week)}}{\text{susceptible population}} \times 100(\%).$$

The binary response is obtained as 1 if the average of the new vaccination rate in 4 weeks (from May 30, 2021 to June 26, 2021) is greater than the

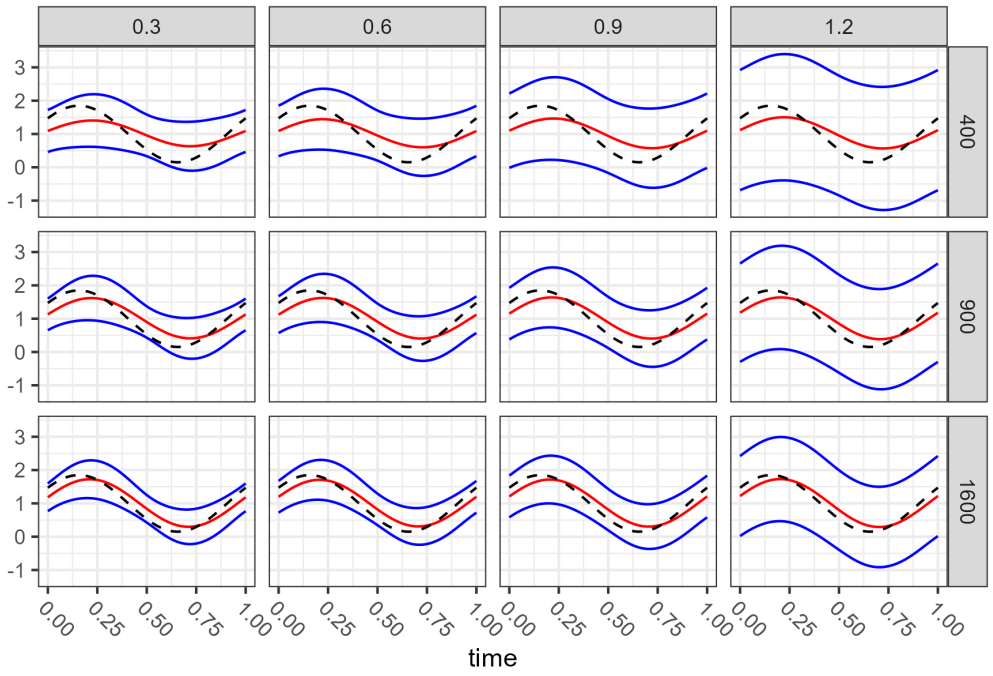

Figure 7: Confidence band of $\beta(t)$ based on the truncation level p selected by BIC_c. The columns represent the spatial parameter η and the rows represent the sample size n. The dotted black line is the true $\beta(t)$, the red line is the average of $\hat{\beta}(t)$, and the blue lines are the average of confidence bands of $\beta(t)$

average overall counties, or 0 otherwise. A map of the responses is shown in Figure 10.

We employ three different time periods for the new positive cases, while we focus on a separate period of 4 weeks for the new vaccination rate. The three time periods for the new positive cases span 20 weeks, 18 weeks, and 16 weeks starting from January 10, 2021. For the new vaccination rate, 4 weeks start from the next day of the last day of the new positive cases. This design allows us to explore potential variations in the relationship between the new infection rate and the new vaccination rate across different time periods or assess its robustness.

5.2. Results

Figure 11 shows the FMSE of each model for the various truncation level $p = 1, \cdots, 10$. Notably, the spatial models, SGLM and SGFLM, consistently

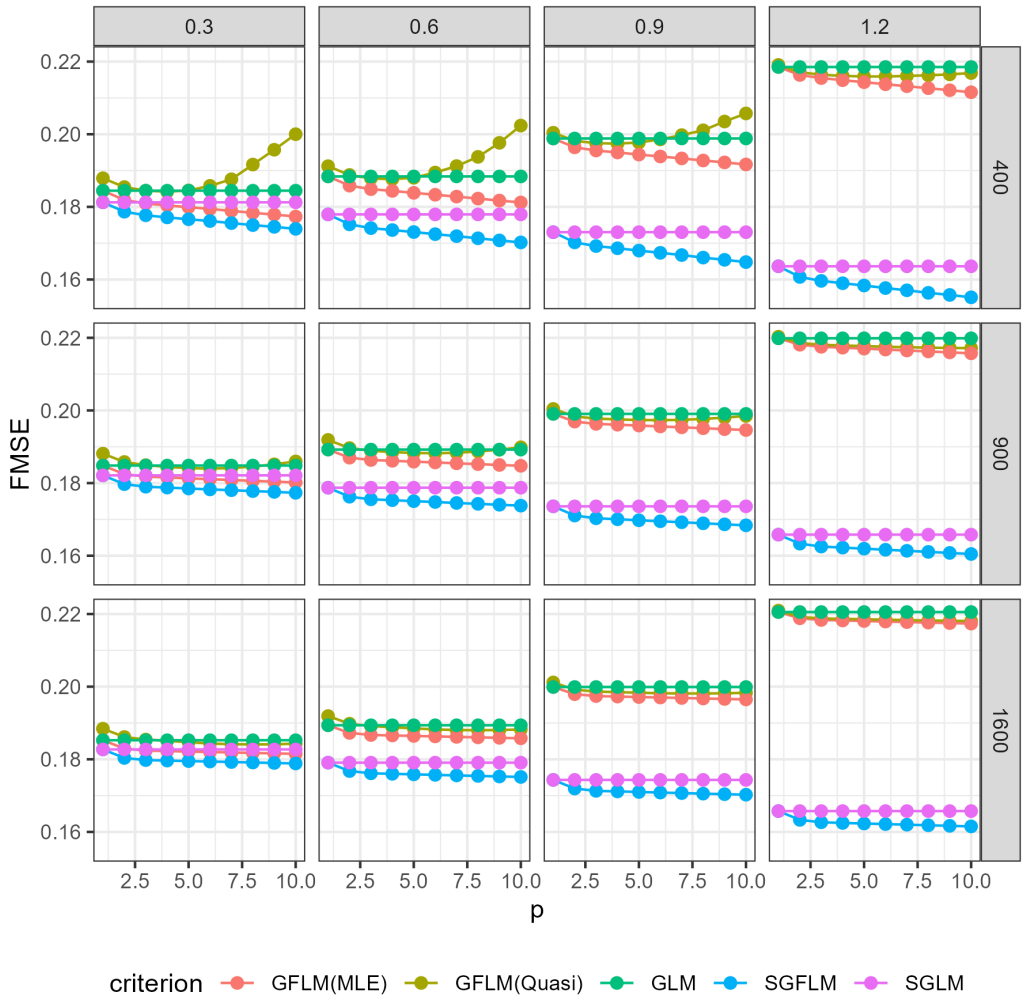

Figure 8: FMSE values depending on the models and/or the estimation methods. Each dot indicates the truncation level $p = 1, \cdots, 10$. Columns indicate the spatial parameter η and rows indicate the sample size n

exhibit lower FMSE values compared to the independent models, GLM and GFLM, across all truncation levels. Among the independent models, it is worth noting that GFLM outperforms GLM in terms of FMSE. GFLM with MLE achieves the smallest FMSE value among all independent models. Similarly, SGFLM demonstrates superior performance in FMSE compared to SGLM.

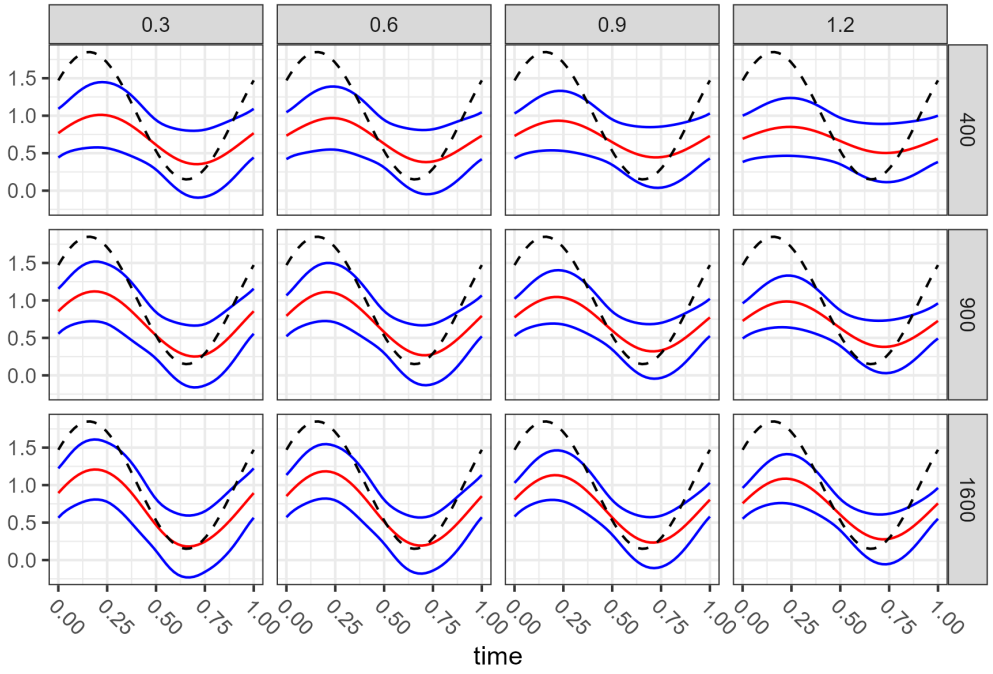

Figure 9: Confidence band of $\beta(t)$ of GFLM based on the truncation level p selected by BIC. The columns represent the spatial parameter η and the rows represent the sample size n. The dotted black line is the true $\beta(t)$, the red line is the average of $\hat{\beta}(t)$, and the blue lines are the average of confidence bands of $\beta(t)$

The truncation level p is selected as 2 by BIC_c, our preferred criterion. The estimated spatial dependence parameter is $\hat{\eta} = 0.748$ with the 95% confidence interval $(0.658, 0.838)$. Moreover, the estimated value for α is $\hat{\alpha} = -2.139$. The estimated function parameter $\hat{\beta}(t)$ and 95% confidence band are presented in the first panel of Figure 12. Based on the confidence band displayed in the first panel of Figure 12, it is evident that the vaccination rate exhibits a positive relationship with the number of positive cases over the past ten weeks. In simpler terms, an increase in the number of positive cases over a ten-week period leads to an increase in the vaccination rate. This relationship is also observed in the different time period, as depicted in the second and the third panels of Figure 12. When using an 18-week time period, we observe that the vaccination rate is influenced by the number of positive cases over the past eight weeks, with a truncation level of $p = 3$. Also, for the 16-week time period, the vaccination rate is affected by the

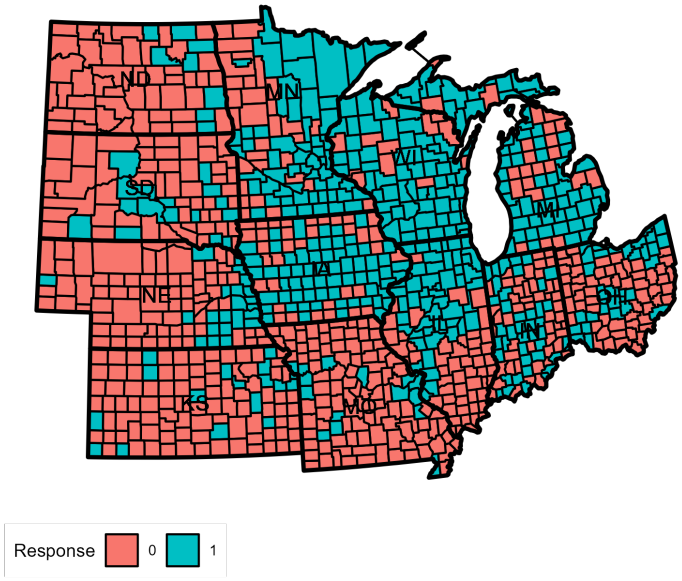

Figure 10: Response variables on the map

number of positive cases over the past four weeks, with a truncation level of $p = 6$. In the case of the 16-week time period, the relatively large truncation level of $p = 6$ compared to the other two time periods (20 weeks and 18 weeks) results in a more intricate and winding confidence band.

Figure 13 displays the discrepancy between the fitted squared error (FSE) of GFLM using MLE and the FSE of SGFLM, specifically when considering the 20-week time period. The FSE is calculated as $(y(\mathbf{s}_i) - \hat{p}(\mathbf{s}_i))^2$, which corresponds to a similar definition of FMSE in Section 3. By examining this figure, we can identify where the spatial model outperforms the independent model. Since the discrepancy is obtained by subtracting the FSE of the spatial model from the FSE of the independent model, a larger discrepancy value indicates that the spatial model performs better than the independent model. Notably, we observe that the superiority of the spatial model is particularly pronounced in urban areas. This implies that individuals in urban areas exhibit more similar behavior compared to those in rural areas. This relationship is also evident in the 18-week and 16-week time periods,

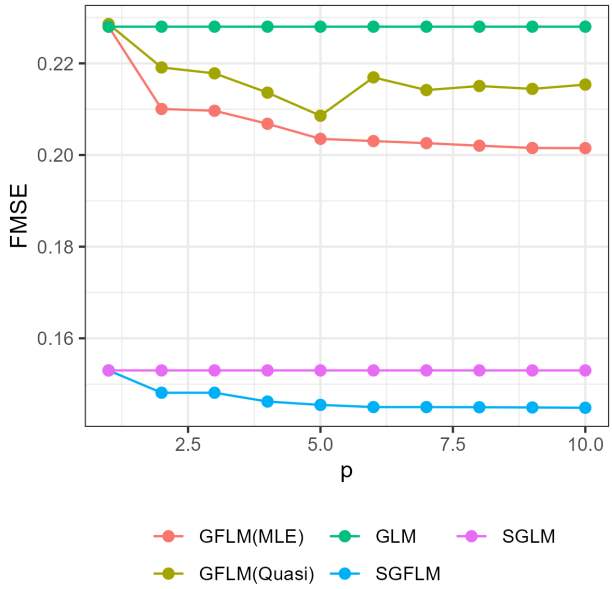

Figure 11: FMSE values depending on the models and/or the estimation methods. Each dot indicates the truncation level $p = 1, \cdots, 10$

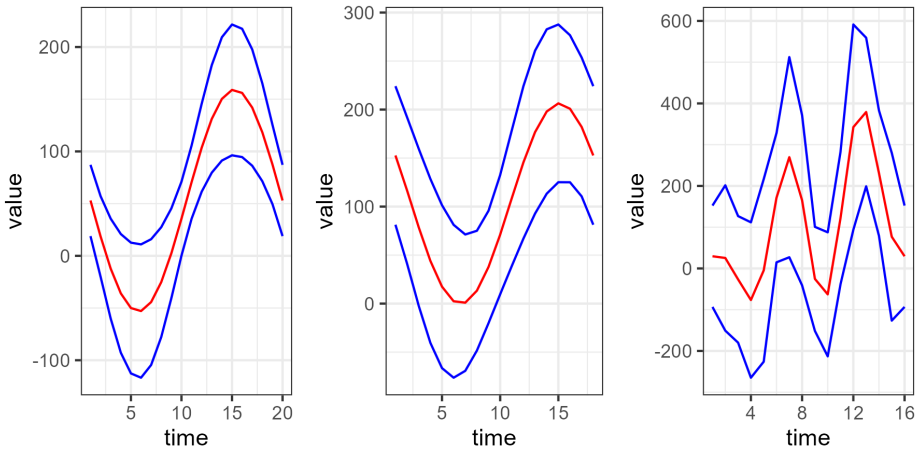

Figure 12: The red line indicates the estimated function parameter $\hat{\beta}(t)$ and the blue lines indicate the confidence band. The panels illustrate the results obtained from an 20 weeks, 18 weeks, and 16 weeks time period from left to right.

further supporting the notion that the superiority of the spatial model is

consistently associated with urban areas.

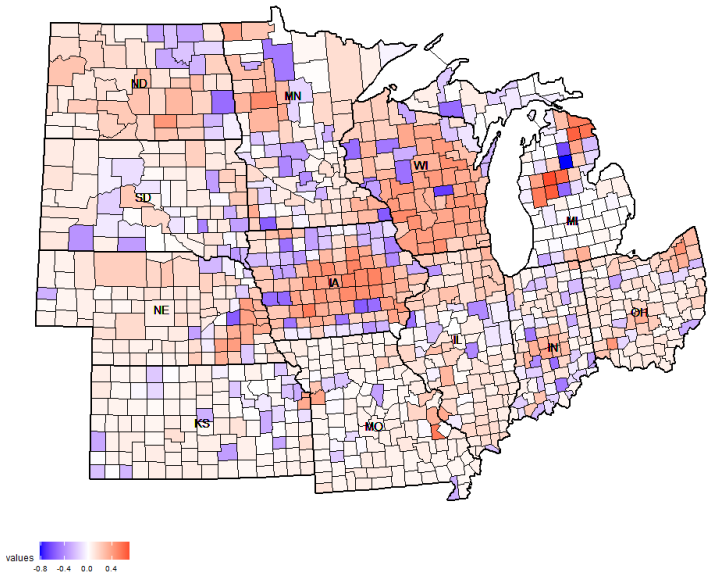

Figure 13: A plot of the discrepancy between the fitted squared error of GFLM using MLE and that of SGFLM when using the 20-week time period

6. Concluding Remarks

We consider the selection of a truncation level for handling a functional covariate in a spatial generalized linear model (SFGLM) which is important in estimation and inference using this model. We examined five criteria for choosing a trunction level, AIC_c, BIC_c, FVE, FMSE, and PE with 1se rule. Based on the analysis of a simulation study we recommend BIC_c as a criterion of choice. BIC_c tends to select lower truncation levels than do the other possible criteria, and this characteristic of the BIC_c criterion is reasonably stable across levels of spatial dependence. The BIC_c criterion also appears to be less influenced by sample size than most of the other possibilities, particularly FVE and FMSE.

In a comparison of models that do or do not contain explicit spatial structure and do or do not include functional covariates, we found that the spatial models outperform the non-spatial models when spatial dependence is present and particularly when it is large. Similarly, models that incorporate

functional covariate behavior outperform those that do not when that structure is present in the data. The proposed SGFLM outperforms all others when the data exhibit both functional covariate behavior and spatial structure. The degree to which this superiority is seen depends on both the degree of spatial dependence and the sample size, as would be expected.

In an application to a problem in which the rate of new vaccinations against COVID is considered as a potentially spatially-structured response and the sequence of new infections over the previous weeks a functional covariate, we demonstrate that SGFLM has smaller fitted mean squared error than models accounting only for spatial structure in responses or that only treat covariate information as a functional process. It does appear that in this problem accounting for spatial structure in responses is perhaps more vital than the incorporation of information from a functional covariate process.

There are several potential extensions to this work. Using a Markov random field as the basis of modeling a spatial response variable should allow a fairly straightforward incorporation of non-isotropic dependencies such as directional dependence. The development of a model that allows the assessment of spatially structured response variables at more than one time point with stretches of functional covariate processes in between assessments of responses is an interesting possibility. Another extension that we find particularly intriguing is that there may be spatial structure exhibited by both a functional covariate process and the regression response variables. Because spatial structure in the covariate process should produce a certain amount of similar structure in responses, determining the relative contributions of covariate process dependence and direct dependence in responses should be a challenging problem as there is likely no unique decomposition of the two.

References

Ahmed, M.S., Broze, L., Dabo-Niang, S., Gharbi, Z., 2022. Quasi-maximum likelihood estimators for functional linear spatial autoregressive models. Geostatistical Functional Data Analysis , 286–328.

Besag, J., 1974. Spatial interaction and the statistical analysis of lattice systems. Journal of the Royal Statistical Society: Series B (Methodological) 36, 192–225.

Besag, J., 1975. Statistical analysis of non-lattice data. The Statistician 24, 179–195.

Gertheiss, J., Maity, A., Staicu, A.M., 2013. Variable selection in generalized functional linear models. Stat 2, 86–101.

Goldsmith, J., Bobb, J., Crainiceanu, C.M., Caffo, B., Reich, D., 2011. Penalized functional regression. Journal of computational and graphical statistics 20, 830–851.

Guyon, X., 1995. Random fields on a network: modeling, statistics, and applications. Springer Science & Business Media.

Jadhav, S., Koul, H., Lu, Q., 2017. Dependent generalized functional linear models. Biometrika 104, 987–994.

Kaiser, M.S., Cressie, N., 2000. The construction of multivariate distributions from markov random fields. Journal of Multivariate Analysis 73, 199–220.

Kim, S., Kaiser, M.S., Dai, X., 2024. Generalized linear models with spatial dependence and a functional covariate. arXiv preprint arXiv:2402.13472 .

Müller, H.G., Stadtmüller, U., 2005. Generalized functional linear models .

Varin, Cristiano, R.N., Firth, D., 2011. An overview of composite likeihood methods. Statistica Sinica 21, 5–42.